Journal of Energy Chemistry 36 (2019) 51–63

Contents lists available at ScienceDirect

Journal of Energy Chemistry

journal homepage: www.elsevier.com/locate/jechem

http://www.journals.elsevier.com/journal-of-energy-chemistry/

Review

Dimethyl ether carbonylation over zeolites

Ensheng Zhan[a,*], Zhiping Xiong[a,b], Wenjie Shen[a,*]

[a] State Key Laboratory of Catalysis, Dalian Institute of Chemical Physics, Chinese Academy of Sciences, Dalian 116023, Liaoning, China
[b] University of Chinese Academy of Sciences, Beijing 100049, China

Dedicated to the 70th anniversary of Dalian Institute of Chemical Physics, CAS, China.

ARTICLE INFO

Article history:
Received 21 January 2019
Revised 7 March 2019
Accepted 10 April 2019
Available online 17 April 2019

Keywords:
DME carbonylation
Zeolites
Mordenite
Acid sites
Reaction mechanism
Deactivation

ABSTRACT

Syngas to ethanol, consisting of dimethyl ether (DME) carbonylation to methyl acetate (MA) over zeolites and MA hydrogenation to ethanol on copper catalyst, has been developed in recent years. DME carbonylation over zeolites, a key step in this new process, has attracted increasing attention due to the high reaction efficiency and promising industrial application. In recent years, continuous efforts have been made on improving the activity and stability of the zeolites. From a mechanistic point of view, DME carbonylation to MA, involving the formation of C–C bond, is achieved via the Koch-type CO insertion into DME within the 8-member ring (8-MR) pores of zeolites, typically HMOR and HZSM-35. The unique geometric configuration of the 8-MR pore endowed the formation of the key intermediate (acetyl, CH_3CO^*), possibly by a spatial confinement of the transition state during CO insertion into the surface O–CH_3 group. This review article summarizes the main progress on zeolite-catalyzed DME carbonylation, including reaction kinetics and mechanism, theoretical calculations, and experimental strategies developed for populating acid sites and engineering pore structure of the zeolites in order to enhance the overall performance.

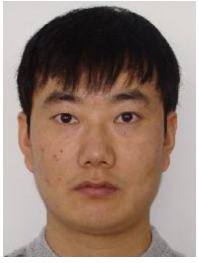

Ensheng Zhan obtained his Ph.D. degree from Dalian Institute of Chemical Physics in 2010. His research focused on the synthesis of zeolites with controlled shape, crystallite size and acid site location, and related application in hydrocarbon conversion and environmental catalysis.

Zhiping Xiong is now a Ph.D. candidate in the Dalian Institute of Chemical Physics. His research topic is the synthesis of 2D zeolites, such as mordenite and ZSM-5, and their application in DME carbonylation reaction.

Wenjie Shen's group research interests involve the synthesis and characterization of catalytic materials with controllable size and morphology from the precursors to the activated catalysts, and the reaction chemistry of hydrogen production form bio-oxygenates, methane conversion, methanol/DME conversion and environmental catalysis.

1. Introduction

Syngas (a mixture of H_2, CO and CO_2) conversion to hydrocarbons and alcohols plays a pivotal role in the utilization of carbon resources such as coal, natural gas/shale gas and biomass [1]. Catalysis for syngas to hydrocarbons, known as Fischer-Tropsch synthesis, mainly deals with the dissociative activation of CO (breaking the carbon-oxygen bond) and controlling the growth of carbon chains in the product; while syngas to alcohols also relates to the non-dissociative activation of CO [2]. With this regard, methanol synthesis represents one of the simplest and most mature syngas conversion processes. Now, mega-ton/year scale methanol synthesis, mostly using the $Cu/ZnO/Al_2O_3$ catalysts, is

* Corresponding authors.
E-mail addresses: eszhan@dicp.ac.cn (E. Zhan), shen98@dicp.ac.cn (W. Shen).

https://doi.org/10.1016/j.jechem.2019.04.015

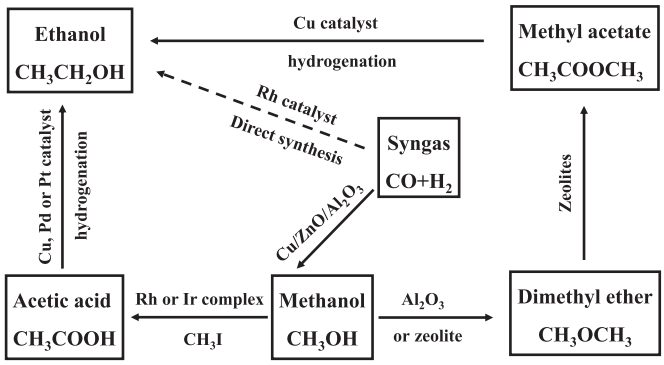

Fig. 1. Reaction routes for syngas conversion to ethanol.

running commercially with methanol selectivity as high as 99.8% and catalyst life of more than 4 years (typically operating at pressures of 5–10 MPa and temperatures of 200–300 °C) [3]. Methanol can be readily converted to dimethyl ether (DME) by a simple dehydration process in large scale, catalyzed by solid acids such as alumina or zeolites. Direct or one-step syngas to DME process over combined $Cu/ZnO/Al_2O_3$ and solid acids has been claimed to be more economically favorable for promoting CO conversion in large scale industrial production, as the dehydration process alleviates the thermodynamic constraints of methanol synthesis [4,5].

Ethanol is considered as a potential alternative transportation fuel and a critical building molecule in chemical industry [6], however, direct conversion of syngas to ethanol remains a long-standing challenge. The main obstacle comes to be the inefficient controlling of the carbon chain growth process. In the syngas to alcohol catalysis, it is well-known that formation of the first C–C bond (C1 to C2 step) is the rate determining step, and the consecutive carbon chain growth is kinetically favored via the β-carbon (defined as the carbon adjacent to the carbon bonded to oxygen) addition mechanism, resulting in depletion of ethanol in the reaction mixture [7]. Cu–Co, Cu–Zn, MoS_2 or Rh catalysts have been demonstrated to be effective for CO hydrogenation to ethanol, but the overall efficiency is limited. Methanol, ethanol, and higher alcohols, together with other oxygenates, are produced simultaneously. Ethanol selectivity over the most pronounced Rh catalysts is usually no more than 50%, which requires a downstream updating process [6]. Industrially, syngas to ethanol is now operated by a two-step process: methanol carbonylation to acetic acid (AA) catalyzed by homogeneous Rh or Ir complexes [8] and hydrogenation of acetic acid or methyl acetate/ethyl acetate (requires additional esterification step) over heterogeneous metal (Cu, Pd and Pt) catalysts to ethanol [9,10]. However, this technology suffers from the harsh operation conditions, the use of expensive noble metals, and the corrosion of acetic acid [10,11].

An alternative approach of syngas to ethanol has been proposed recently. It consists of DME carbonylation over zeolites to methyl acetate (MA) and MA hydrogenation to ethanol over Cu catalysts (Fig. 1) [12–15]. The key reaction, DME carbonylation to MA with the formation of C–C bond, simply catalyzed by zeolites, represents a halide-free, non-noble metal, and highly efficient process. Moreover, methyl acetate serves as the intermediate to produce ethanol via hydrogenation, avoiding the use of acetic acid that is strongly corrosive.

2. Methanol/DME carbonylation

2.1. Homogeneous catalysts

Methanol carbonylation is a homogeneous process using Rh (Monsanto process) or Ir (BP Cativa^{TM} process) catalysts. As these metal complexes do not activate methanol directly, the more reactive methyl iodide (CH_3I) must be used as an essential promoter [8]. Within such a catalytic recycle, hydrogen iodide (HI) is involved to convert methanol into methyl iodide. Moreover, water (10–15 wt%) is added to the reaction system to prevent the catalysts from precipitation and maintain the activity, which makes the process more corrosive and toxic [16]. Meanwhile, this process suffers from product/catalyst separation. Therefore, developing iodide-free heterogeneous catalysts for methanol carbonylation, with competitive activity and selectivity to the homogeneous catalyst, has attracted intensive attentions during the past decades.

2.2. Heterogeneous catalysts

A key step for methanol/DME carbonylation is to break the C–O bond. The C–O bond energy is 385 kJ mol^{-1} in methanol, and 352 kJ mol^{-1} in DME, which is much stronger than the C–I bond (239 kJ mol^{-1}). Inspired by the strong acid catalyzed carbonylation of alcohols, namely the 'Koch reaction' [17], two types of solid acids have been developed for methanol/DME carbonylation: zeolites and Ir/Rh exchanged heteropolyacids, as shown in Table 1.

2.2.1. Zeolites

In 1984, a pioneer work of Fujimoto et al. described the use of zeolites (HY, HZSM-5, and HMOR) as well as Cu-modified zeolites (Cu/HZSM-5 and Cu/HMOR) for methanol carbonylation [18]. Although the yield of acetyls (AA and MA) was very low (<1%, Table 1), because DME was formed as the major product, these experiments demonstrated the occurrence of methanol carbonylation over zeolites. In 1996, researchers from BP Chemicals re-examined the performance of HMOR and Cu/HMOR for methanol carbonylation, and a notable space time yield of acetyls up to 0.3 g g_{cat}^{-1} h^{-1} was obtained over Cu/HMOR [19]. An interesting phenomenon with respect to the variations in the selectivity of the products on both catalysts was observed during reaction (350 °C, 1.0 MPa, CO/methanol=10/1). Gasoline-range hydrocarbons were the major product at the initial stage, indicting the occurrence of methanol to gasoline (MTG) reaction; acetyls with a selectivity of 60%–80% were formed after 6 h on Cu/HMOR and 15 h over HMOR; while DME became dominant after 20–25 h with a significant drop in the selectivity of acetyls. It was accordingly proposed that the active sites for methanol carbonylation was very limited, as compared to those for MTG reaction; methanol carbonylation reaction became dominate only after the active sites for the MTG reaction were blocked by coke deposition.

2.2.2. Heteropolyacids

Ir/Rh exchanged heteropolyacids were developed by researchers from Union Carbide in 1994 for carbonylation of methanol/DME [20]. The most interesting result concerned the crucial role of the exchanged noble metals. Bare heteropolyacids yielded only small amount of MA (1%–8%) in methanol carbonylation with DME as the main product (more than 90%). While the yield of MA increased to 30%–40% upon ion-exchange with Ir or Rh. Moreover, MA was the only product in DME carbonylation on the $RhW_{12}PO_{40}/SiO_2$ catalyst under mild conditions (225 °C, 0.1 MPa, CO/DME = 3, GHSV = 900 h^{-1}). $RuW_{12}PO_{40}/SiO_2$ was also tested for DME carbonylation, but the selectivity for MA was less than 20%, while the selectivity of hydrocarbons was over 80% [23]. In addition, Ir or Rh loaded on $Cs_xH_{3-x}W_{12}PO_{40}$ ($1.5 \le x \le 2$) were found to be more active than those loaded on the $H_3W_{12}PO_{40}$ counterpart, possibly due to the higher amount of surface protons exposed as active sites that benefited from the lager surface area of the salt [21,24]. Similarly, dispersing heteropolyacids ($H_3PW_{12}O_{40}$, $H_3PMo_{12}O_{40}$ and $H_4SiW_{12}O_{40}$) on mesoporous materials (SBA-15) were found to enhance the density of acid sites that are accessible to the reactants and thus the activity of DME carbonylation [25]. Investigations on the reaction mechanism, by using solid-state

Table 1. Heterogeneous catalysts for methanol/DME carbonylation.

Catalyst	Reaction conditions[a]	Conversion (%)	Selectivity (%)		Reaction rate[b] ($g\ g_{cat}^{-1}\ h^{-1}$)	Ref.
			AA	MA		
HY	200 °C, 1.0 MPa, CO/MeOH = 1	n/a	trace	0.3	n/a	[18]
HMOR		n/a	0.2	0.01	n/a	
Cu-HMOR		n/a	0.28	0.37	n/a	
Cu-HMOR	350 °C, 1.0 MPa, CO/MeOH = 10	>90	~70		0.3	[19]
$RhW_{12}PO_{40}/SiO_2$	225 °C, 0.1 MPa, CO/MeOH = 10	83	0	34	0.065[c]	[20]
$IrW_{12}PO_{40}/SiO_2$		92	0	40	0.076[c]	
$RhW_{12}PO_{40}/SiO_2$	225 °C, 0.1 MPa, CO/DME = 3	16	0	100	0.1[c]	
$RhCs_2H_1W_{12}PO_{40}$	200 °C, 1.0 MPa, CO/DME = 10	n/a	n/a	96	0.13	[21]

[a] CO/Methanol or CO/DME in molar ratio.
[b] Reaction rates estimated from the reported feed gas space velocity and product yield.
[c] Space time yield (STY) in $g\ mL_{cat}^{-1}\ h^{-1}$.

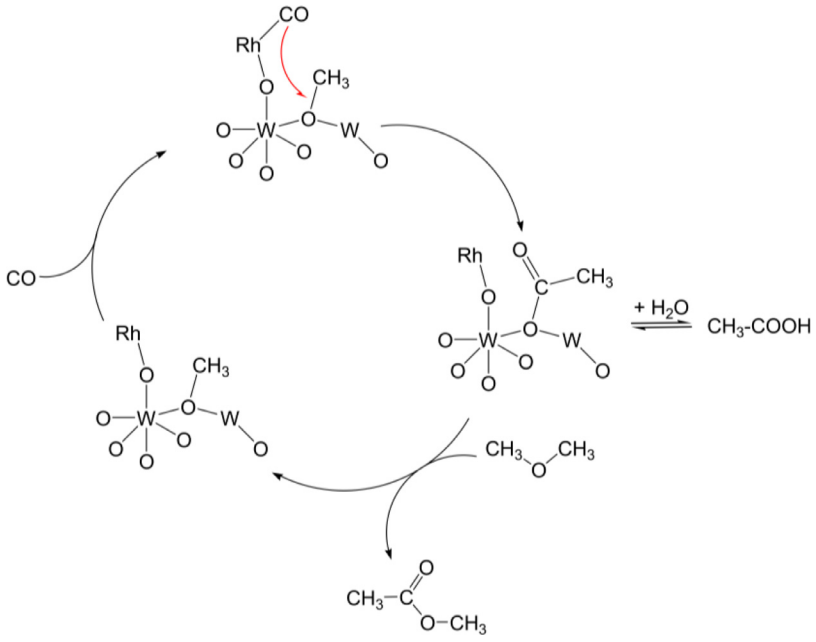

Fig. 2. Proposed mechanism for DME carbonylation on $Rh/Cs_2HPW_{12}O_{40}$ [22].

NMR [22,26–28] and IR [29], revealed that, upon adsorption of methanol/DME, surface methoxy group was formed on the acidic OH group over the heteropolyacids, and CO insertion into the CH_3–O bond resulted in the formation of acetate group attached to the Keggin anion. The promoting role of the noble metals was to adsorb CO from the gas phase and then transfer it to the surface CH_3–O bond to form acetyls (Fig. 2) [22].

Despite these efforts in heterogeneous carbonylation of methanol/DME, the overall efficiency is still far below the homogeneous system. In 2006, Iglesia et al. reported that DME carbonylation over zeolites, typically HMOR, HFER, and HZSM-5, had much higher reaction rates than methanol carbonylation [30,31]. Especially, HMOR gave the excellent selectivity (> 99%) towards MA at 150–190 °C with a feed gas composition of 0.93 MPa CO and 20 kPa DME. DME is preferential to methanol just because water, generated from dehydration of methanol, may adsorb competitively at the sites for CO binding, inhibiting CO reaction with the adsorbed methyl ($-CH_3$). This work put new insights into the new, yet old reaction, and thereafter great efforts have done on elaborating the reaction mechanism and developing zeolites with novel structure and high performance [12,13,32–41].

3. DME carbonylation over zeolites

To date, zeolites that could show promising activity for DME carbonylation are those containing 8-member ring (MR) pores with appropriate pore size and geometric configuration. Among them, HMOR and HFER are the two most studied categories, as shown in Table 2. At reaction temperatures between 150 and 300 °C, HMOR is the most active and selective system, while HFER is also highly selective for MA but its activity is about an order of magnitude lower than HMOR. As shown in Fig. 3, the topology structure of MOR is characterized by parallel 12-MR (6.5 × 7 Å) and 8-MR (2.6 × 5.7 Å) channels along the c-axis, which are interconnected by 8-MR side-pockets (3.4 × 4.8 Å) along the b-axis. FER contains 10-MR channels (5.4 × 4.2 Å) along the c-axis with intersecting 8-MR channel (4.8 × 3.5 Å) along the b-axis, and 6-MR channels running parallel to the c-axis, where the intersection of an 8-MR and a 6-MR channel creates a $[8^26^86^45^8]$ cage, known as "ferrierite cavity" that is accessible only via the 8-MR windows [48]. Although also containing 8-MR pores, other zeolitic topologies, such as OFF, CHA, ECR and MAZ, did not show satisfied performance for DME carbonylation [42], possibly because the acid strength or the

Table 2. DME carbonylation over zeolite catalysts.

Catalyst[a]	Reaction conditions[b]	MA Selectivity (%)	Reaction rate[c] ($g\ g_{cat}^{-1}\ h^{-1}$)	Ref.
MOR (10)	165 °C, 1.0 MPa, CO/DME/Ar = 93/2/5	99	0.1	[31]
	190 °C, 1.0 MPa, CO/DME/Ar = 93/2/5	96	0.3	
FER(34)	186 °C, 1.0 MPa, CO/DME/Ar = 93/2/5	94	0.014	
MFI(6)	186 °C, 1.0 MPa, CO/DME/Ar = 93/2/5	14	0.01	
FAU(3)	191 °C, 1.0 MPa, CO/DME/Ar = 93/2/5	<1	<0.003	
FER(8.1)	200 °C, 1.0 MPa, $CO/DME/N_2/He = 5/50/2.5/42.5$	96	0.02	[33]
MOR(5.5)	180 °C, 1.5 MPa, $CO/DME/N_2 = 95.5/3/1.5$	98	0.27(4.5)	[35]
MOR(11.8)	200 °C, 1.5 MPa, CO/DME = 49/1	>95	0.47	[37]
FER(11.4)	220 °C, 2.0 MPa, $CO/DME/N_2 = 45/5/50$	94.7	0.05	[39]
OFF(10)	180 °C, 7.0 MPa, $CO/DME/H_2/N_2 = 64/5/15/16$	n/a	0.055(19.6)[d]	[42]
CHA(7.3)		n/a	0.013(19.7)[d]	
ECR(7.8)		n/a	0.025(16.0)[d]	
MAZ(7.7)	250 °C, 7.0 MPa, $CO/DME/H_2/N_2 = 64/5/15/16$	n/a	0.006(49.9)[d]	
FER(12.9)	220 °C, 2.0 MPa, CO/DME = 10/1	98	0.087	[43]
MOR(22)	300 °C, 1.0 MPa, $CO/DME/H_2 = 76/5/19$	70	0.8(8)	[44]
MOR(13.5)	200 °C, 1.0 MPa, $CO/DME/N_2/He = 5/50/2.5/42.5$	99	0.07(4)	[45]
ETL(10)	220 °C, 1.0 MPa, $CO/DME/Ar = 4.13/92.84/3.03$	>90	0.043	[46]
HEU	210 °C, 3.0 MPa, CO/DME = 1/30	>99	0.0545	[47]

[a] Numbers in the bracket are the Si/Al ratios.
[b] Gas composition in molar ratio.
[c] Reaction rates estimated from the reported feed gas space velocity and product yield, numbers in the bracket are time on stream at which the data were collected.
[d] Space time yield (STY) in $g\ mL_{cat}^{-1}\ h^{-1}$.

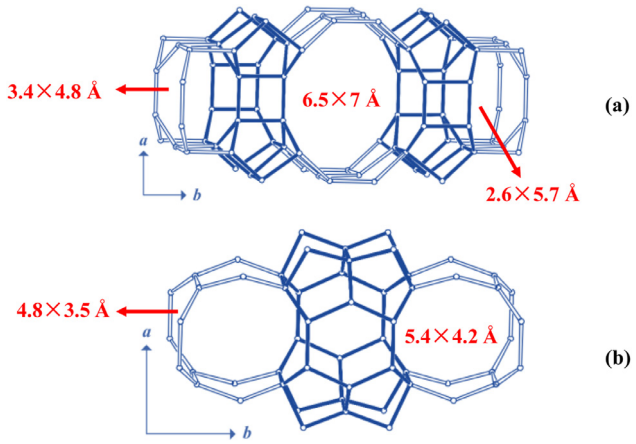

Fig. 3. Framework images of MOR (a) and FER (b) zeolites viewed along [001] direction.

configuration of the 8-MR pores in these zeolites is not compatible for the activation of DME molecule and the accommodation of the reaction intermediates. Quite recently, two types of zeolites, EU-12 [46] and clinoptilolite [47] with ETL and HEU topologies, respectively, were found to show moderate activity and high stability in DME carbonylation; the MA formation rates approached to that of FER zeolites (Table 2). The unique performance of these zeolitic topologies would benefit in-depth understanding of the structure-reactivity relationship of zeolites in DME carbonylation.

Transition metals (Cu, Co, Zn, Ni, Ag and Fe) are typically adapted to enhance the catalytic activity of HMOR for DME carbonylation (Table 3). The chemical principle is that transition metals have strong ability for CO adsorption and activation, which facilitates CO insertion into the methyl group adsorbed on a vicinal acid site of HMOR. Cu, Ni, Co, Zn modified HMOR catalysts, prepared either by impregnation or ion-exchange, showed higher activity or stability than the parent HMOR in DME carbonylation, with Cu as the most efficient promoter [38,44,51–58]. Interestingly, co-addition of Cu and Zn to HMOR resulted in more dramatic improvement in both activity and stability as compared to the addition of either Cu or Zn individually. For instance, a Cu-Zn/HMOR catalyst provided a 6-fold higher overall yield of MA and a 4-fold lifetime by referencing to the Cu/HMOR [38]. A combined IR, UV-vis and theoretical modeling study indicated that monometallic exchange of Cu and Zn resulted in their location at T1 and (T3+T4) sites of HMOR framework, respectively; while Cu promoted the preferable location of Zn from T3 site to T4 site when they are co-exchanged. The enhanced stability of the Cu–Zn/HMOR catalyst was ascribed to block the T4 sites which was assumed to be responsible for the formation of coke precursor [56,57]. Introducing Fe into the framework T sites of HMOR, during the hydrothermal process, was also reported to enhance the catalytic activity, and especially stability, in DME carbonylation. It was proposed that Fe decreased the acid strength and density in the 12-MR channel of HMOR and thus mitigated carbon deposition [53].

4. Reaction mechanism

4.1. The catalysis cycle

The reaction mechanism of DME carbonylation over zeolites has been intensively investigated by various techniques, such as kinetic and isotopic-exchange experiments [59], IR [60,61], solid-state NMR [62,63] and theoretical calculations [32]. It is now generally acknowledged that DME initially reacts with the acid site (OH) on the zeolite framework, forming adsorbed methyl and releasing methanol simultaneously (induction period, Fig. 4); then CO inserts into the C–O bond between the adsorbed methyl group

Table 3. DME carbonylation over transition-metal-modified HMORs.

Catalyst[a]	Reaction conditions[c]	MA selectivity (%)	Reaction rate[d] ($g\ g_{cat}^{-1}\ h^{-1}$)	Ref.
MOR(6.5)	210 °C, 1.0 MPa, $CO/DME/H_2/He = 50/2.4/2.9/44.7$	96	0.213	[38]
3.21 wt%Cu-MOR		94	0.206	
3.05 wt%Zn-MOR		95	0.217	
0.57 wt%Cu-2.47 Zn wt%-MOR		98	0.24	
MOR(22)	300 °C, 1.0 MPa, $CO/DME/H_2 = 76/5/19$	70	0.8(8)	[44]
2.4 wt% Cu-MOR		80	0.96(8)	
MOR(10)	300 °C, 5.0 MPa, 5%DME, $H_2/CO = 1/4$	85	0.033[e]	[49]
Cu(55)-MOR[b]		93	0.17[e]	
Ag(55)-MOR[b]		95	0.16[e]	
MOR(10)	300 °C, 3.0 MPa, $DME/CO/H_2/N_2/He = 4.9/63.1/15.8/14.8/1.4$	n/a	0.086[f]	[50]
Cu(55)Pt(1)-MOR		n/a	0.201[f]	
Cu(55)Pt(10)-MOR		n/a	0.216[f]	
MOR(9)	210 °C, 1.8 MPa, $CO/DME/N_2 = 38/2/3$	97.3	0.35	[51]
1.74 wt%Cu-MOR		99.6	0.62	
1.30 wt%Ni-MOR		98.7	0.4	
1.36 wt%Co-MOR		99.4	0.47	
1.67 wt%Zn-MOR		97	0.35	
1.64 wt%Ag-MOR		94.3	0.22	
MOR(8.2)	200 °C, 1.5 MPa, $CO/DME = 47/1$	>98	0.24	[52]
3.35 wt%Cu-MOR		>98	0.32[g]	
6.16 wt%Cu-MOR		>98	0.43[g]	
10.18wt%Cu-MOR		>98	0.39[g]	
MOR(7.5)	200 °C, 3.0 MPa, $CO/DME/H_2 = 35/5/60$	98	0.17(2)	[53]
0.89%Fe-MOR		98	0.19(2.5)	
MOR(13.5)	200 °C, 1.0 MPa, $CO/DME/H_2 = 76/5/19$	>98	0.07(5)	[54]
0.98 wt%Co-MOR		>98	0.16(8)	

[a] Numbers in the bracket after the zeolite are the Si/Al ratios.
[b] Numbers in the bracket after the metal are the metal/Al ratios.
[c] Gas composition in molar ratio.
[d] Data taking at maximum activity unless otherwise specified, numbers in the bracket are hours of time on stream at which the data was derived.
[e] Space time yield (STY) of the total acetyls (AA and MA) in ($g\ mL_{cat}^{-1}\ h^{-1}$), average data from 27.8 to 56.3 h.
[f] Space time yield (STY) of the total acetyls (AA and MA) in $g\ mL_{cat}^{-1}\ h^{-1}$, average data from 92.2 to 102.2 h.
[g] Catalyst reduced at 300 °C for 3 h before test.

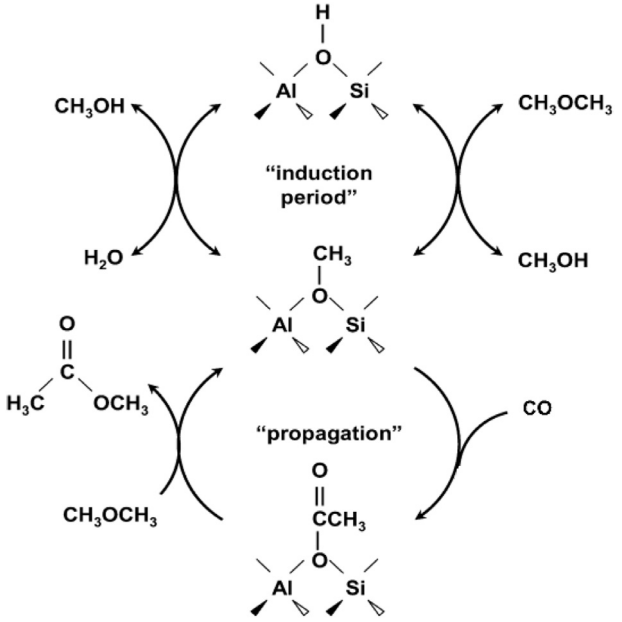

Fig. 4. Proposed mechanism for DME carbonylation over zeolites [59].

and the framework oxygen of the zeolite pore wall, forming the adsorbed acetyl group; finally the acetyl group reacts with another DME molecule to form MA and regenerates another adsorbed methyl group simultaneously (propagation, Fig. 4).

Kinetic studies over HMOR showed that MA formation rate is proportional to CO pressure (0–0.93 MPa) but independent of DME partial pressure (0.8–8 kPa), which indicated that the active sites were saturated with adsorbed species derived from DME and the rate-determining step may involve the reaction of CO, either in gas phase or adsorbed, with the adsorbed species derived from DME [30]. In situ IR studies confirmed that DME dissociatively adsorbed as methyl group ($-CH_3$) by replacing proton (H^+) on the Brønsted acid sites, resulting in the appearance of induction period, during which methanol was formed [59–61]. As shown in Fig. 5, the negative band around 3600–3800 cm^{-1} after DME adsorption indicated the occupation of the O–H sites, and the concurrently appearance of the bands at 2978 cm^{-1} (antisymmetric C–H stretching) and 2868 cm^{-1} (symmetric C–H stretching) confirmed the formation of methyl group ($-CH_3$); the other absorption bands were ascribed to the hydrogen bond interaction of DME with the Brønsted acid sites [61]. Isotopic exchange experiments by reaction of $^{13}CH_3O^{13}CH_3$–^{12}CO–$^{12}CH_3O^{12}CH_3$ confirmed that the carbonyl group in MA originates from CO, while the formation of methyl acetate in a mixture of CH_3OCH_3–CO and CD_3OCD_3–CO excluded the cleavage of the C–H bond [59].

Water is detrimental for acetyl formation during DME carbonylation. Control experiment showed that addition of water (1.1 kPa) to a DME-CO mixture (26 kPa DME, 123 kPa CO) dramatically decreased MA formation rate from 0.034 to 0.0024 mol $(g_{\text{-atom Al}})^{-1}\ h^{-1}$ at 150 °C, but enhanced methanol formation rate by a factor of 14 via DME hydration [59]. However, MA formation rate remained proportional to CO pressure and independent of DME pressure even in the presence of water, indicating that water does not compete with methyl adsorption. Instead, water may inhibit reaction rate either by adsorbing competitively with CO or by decreasing

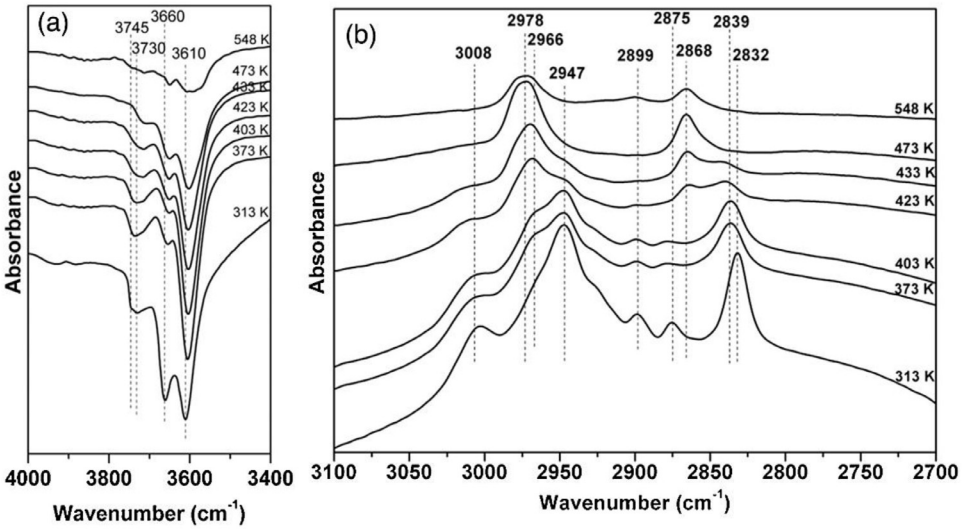

Fig. 5. In situ IR spectra of in O–H (a) and C–H (b) regions of DME adsorption on HMOR [61].

the reactivity of surface methyl groups toward CO molecule. Methanol adsorption resulted in the formation of water, while DME adsorption forms methanol but no water molecule is involved under steady-state DME carbonylation. Therefore, it becomes understandable that both methanol and DME formed methyl as the same adsorbed species on the Brønsted acid site, but methanol carbonylation showed very low activity as compared to DME carbonylation. It should be noted that kinetic and spectroscopic studies did not support the involvement of chemisorbed CO during DME carbonylation over HMOR. Detailed mechanism about how water decreased the reaction rate of surface methyl with CO is still unclear from experimental investigations. Theoretical calculations have predicted that the reaction of water with surface methyl is kinetically favorable as compared with CO insertion; the former involves an activation energy below 80 kJ mol^{-1} on most T sites, while the latter requires an activation energy of at least 100 kJ mol^{-1} on T3-O33 site [32]. It has also been proposed that water molecules tend to form clusters [64] that block the 8-MR pockets (the solely active site for DME carbonylation over HMOR) and thus inhibits DME carbonylation at low temperatures [65].

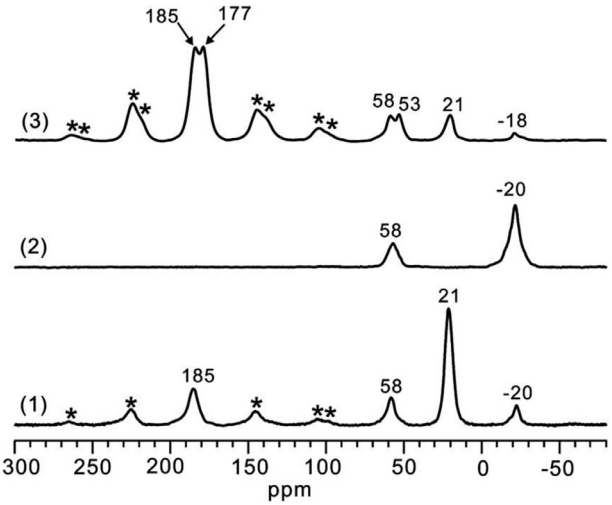

Fig. 6. ^{13}C CP/MAS NMR spectra of product formed from (1) reaction of ^{13}CO and $^{13}CH_3I$ on HMOR at 200 °C for 1 h; (2) reaction of ^{13}CO and $^{13}CH_3I$ on HMOR-12MR at 200 °C for 0.5 h; (3) reaction of ^{13}CO and $^{13}CH_3I$ and DME on HMOR at 200 °C for 1 h. The spinning rate is 4 kHz. The asterisks denote spinning side bands [62].

4.2. C–C formation

CO insertion is regarded as the rate-determining step for DME carbonylation. Here, only methyl group adsorbed in the 8-MR channel of zeolites, like HMOR and HFER, is uniquely reactive toward CO insertion, while those adsorbed in 12-MR and 10-MR channels of HMFI, HBEA, and HFAU give undetectable carbonylation rates [30,59]. MA formation rates showed a linear relationship with the number of acid sites in the 8-MR pores of HMOR and HFER [66,67]. In-situ ^{13}C solid-state NMR evidenced that the transformation of surface methyl to acetyl occurred in the 8-MR channel of HMOR [62]. As shown in Fig. 6, at 200 °C, surface acetyl species (185 ppm) formed by reaction of ^{13}CO and $^{13}CH_3I$ was unambiguously identified over H-MOR (Fig. 6-1), while only surface methoxy group (58 ppm) was formed over HMOR with acid sites located only in the 12-MR pore (HMOR-12, Fig. 6-2). The reaction of ^{13}CO, $^{13}CH_3I$ and DME on HMOR resulted in the formation of methyl acetate in the 12-MR pores (177 and 53 ppm, Fig. 6-3), which was ascribed to the initial formation of acetyls in the 8-MR pores and their further diffusion to the 12-MR pores.

The distinct function of 8-MR pores/channels that favored methyl to acetyl transformation, among other reaction pathways (such as to hydrocarbons), inspires a reconsideration of the well-known concepts of 'restricted transition-state selectivity' and 'confinement effect' in zeolite catalysis. The former refers to the size exclusion effect of transition state that can be formed during reaction, which is determined by the size and configuration of the zeolite pores or cavities [68]. The confinement effect is related to the phenomenon that only certain guest molecule can be accommodated by zeolite pores with specific size and shape, involving several types of interactions: columbic interaction, coordination or vander Waals type weak electronic interactions [69]. Both concepts intrinsically described the strong effect of zeolite local environment, from both topological and electronical point of views, on the transition states or adsorbed species (intermediates) that may influence the reaction pathways and the conversion rates.

The special interaction (solvation effect) that the 8-MR ring pores, especially the 8-MR side pocket of HMOR, imparted to the transition state and reaction intermediates, can be interpreted from two perspectives. First, for reactions via cationic transition states, the nonlocal solvation effect of zeolite framework oxygens at pore walls can decrease the activation energy by charge-compensating with the cationic species. During CO insertion, the more effective

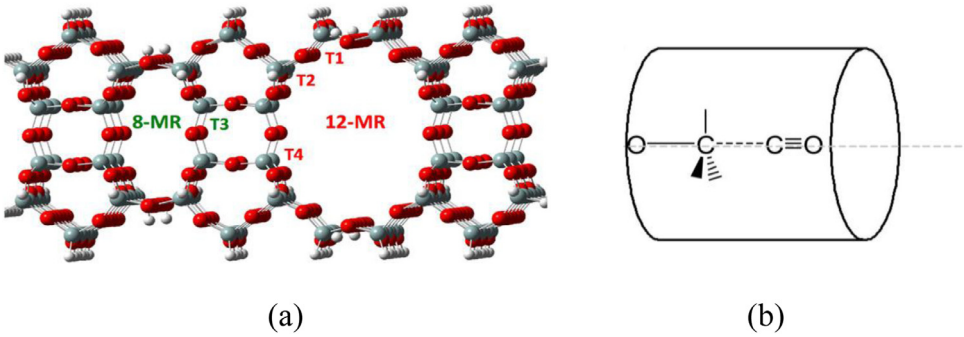

Fig. 7. (a) T sites in the MOR framework [56] and (b) schematic illustration of the orientation of the $O_{framework}$–CH_3 bond at the T3-O33 position [32].

Table 4. Calculated activation energies (kJ mol^{-1}) at the DFT and DFT-D (dispersion force considered) levels on T3 and T4 positions in HMOR [65].

Position	T3 (8-MR)		T4 (12-MR)	
Computational level	DFT	DFT - D	DFT	DFT - D
Z-H + DME → Z-CH_3 + CH_3OH	100.9	−25.5	62.8	7.5
Z-CH_3 + CO → Z-$COCH_3$	99.6	54	100.7	80.4
Z-$COCH_3$ + DME → Z-CH_3 + acetate	271.3	208.5	−15.9	−82.9

van der Waals contacts of the ionic transition state with the framework O-atoms of the small 8-MR voids make the adsorption enthalpies more negative, lowering the activation energy [66,70,71]. Second, the power of the solvation effect also depends on the positioning of the "solvent" within zeolite channels. Specifically, DFT calculations showed that the T3-O33 site (Fig. 7a) endowed adsorption of methyl to adopt an unusual orientation that is parallel to the cylinder axis; such an orientation perfectly fitted the attack of linear CO through a linear transition state that follows the orientation of the O(Z)–CH_3 bond (Fig. 7b). In contrast, the transition state for the attack of DME on the methyl group to form hydrocarbons is highly destabilized, leading to a higher activation energy [32]. This explains the high selectivity of MA in DME carbonylation on HMOR. Furthermore, when dispersion interactions are considered in the theoretical calculations, a more profound lowering of activation energy was established on T3 site (in the bottom of 8-MR side pockets, Fig. 7a) than T4 site (in the intersection between the 12-MR channel and the 8-MR side pocket, Fig. 7a) of HMOR, as shown in Table 4 [65]. These results agreed with the experimentally observed higher activity and selectivity for acetyl formation inside the 8-MR channel of HMOR.

CO insertion to form surface acetyl on HMOR was proposed to involve a transition state with cationic characteristics [66,70,71,73], but the cationic species (acylium cation or acetyl carbocation) has not yet been identified experimentally. DFT calculations predicted that the formation of surface acetyl may contain three elementary steps, as shown in Fig. 8 [72]. Formation of acetyl carbocation in the first step (i.e. the rate-determining step) had an energy barrier of 99.2 kJ mol^{-1}, which is consistent with the activation energy (99.6 kJ mol^{-1}, without considering dispersion force [32]) for the formation of surface acetyl. Acetyl carbocation then transformed to ketene (CH_2=C=O) that is physisorbed on the Brønsted acid site, and finally to adsorbed acetyl species. According to these results, both acylium cation to ketene and ketene to acetyl involved very low energy barriers, with activation energies below 20 kJ mol^{-1}, indicating that the transformation from acylium cation to adsorbed acetyl is very fast. Isotopic-exchange experiments have proved the existence of ketene, by introducing D_2O to the reaction stream and detecting the signal of CH_2DCOOD (m/z = 62) [72].

The adsorption of DME and CO as well as their reaction behavior on HFER has also been investigated by theoretical calculations.

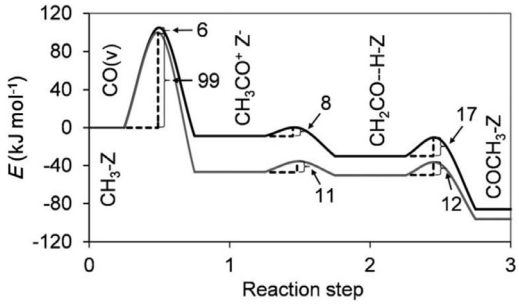

Fig. 8. Reaction pathways for the formation of acetyl from a methyl group and CO within the 12-MR pore on T1-O4 (black line) and the 8-MR pore on T3-O3 (gray line). Reaction steps: 0. CO in vacuum, methyl group on the zeolite; 1. acetyl carbocation and negatively charged zeolite; 2. ketene physisorbed onto a Brønsted acid site; 3. acetyl group on zeolite [72].

Both CO and DME preferentially adsorbed in the 6-MR zone of 8-MR channel, regardless of the acid site density [74]. Formation of acetyl intermediate by CO attack to surface methyl group was kinetically favored on T2 and T4 sites located in the 6-MR zone of 8-MR channel. Experimentally, the higher MA formation rate over a FER@FER (FER zeolite obtained by a FER seed assisted recrystallization process) catalyst with less defect sites than the original FER, has been ascribed to the abundance of stable T2 sites [75,76]. Moreover, theoretical calculation has demonstrated that the activation energies for the reactions of water and CO with surface acetyl on the T2-O5 site were comparable, indicating that DME carbonylation over FER might be less likely to be suppressed by the competitive adsorption of water, unlike the case for HMOR [77]. However, experimental data on the effect of water on DME carbonylation over HFER is unavailable by far.

4.3. MA formation

The reaction of DME with surface acetyl to form MA on the T3 site inside the 8-MR pores of HMOR is still under debating. DFT calculations indicated that direct reaction of DME with surface acetyl is prohibited on the T3 site, because the activation energy is as high as 208.5 kJ mol^{-1} (Table 4) [65]. This is much higher than that for the CO insertion step (54 kJ mol^{-1}, by considering dispersion force), which is generally viewed to be the rate-determine step of DME carbonylation. Accordingly, the formation of MA is proposed to originate from the reaction of methanol (generated by the reaction of DME with a Brønsted acid site) with surface acetyl. However, it was also theoretically predicted that direct reaction of DME with surface acetyl on the T3 site is possible *via* the formation of a CH_3–MA^+ complex, because the activation energy (84.8 kJ mol^{-1}) is slightly lower than that for the CO in-

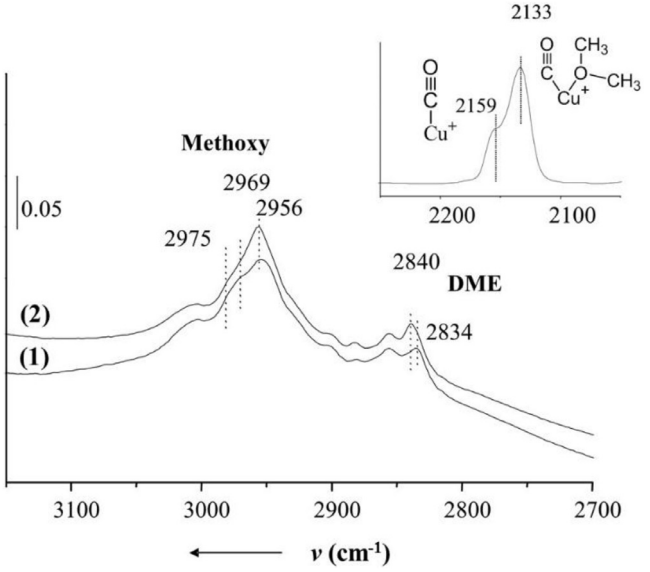

Fig. 9. IR spectra of HMOR (1) and Cu-HMOR (2) upon CO/MeOH co-adsorption at 200 °C. The inset shows the carbonyl stretching vibration associated to the Cu-HMOR [79].

sertion (99.2 kJ mol^{-1}) [78]. Overall, the reaction of methanol with surface acetyl, with activation energy far below that for DME on the T3 site of HMOR, seems to be more favorable from theoretical calculations [65,78], but experimental data is still lack. One interesting experiment has indicated that the formation rate of MA decreased at high MA partial pressures, implying an inhibition effect of MA on DME carbonylation [78]. This phenomenon has not been well addressed in previous studies but is critically important for industrial operation which usually run at high DME conversion level at which the impact of MA would be very significant. This inhibition effect was presumably ascribed to MA adsorption on the acid site within the 8-MR side pocket and block CO insertion to surface methyl, but detailed mechanism is equivocal.

4.4. Role of transition metals

Cu-HMOR represents the most intensively studied case regarding the working mechanism of the promotional effect by transition metals. A comparative study of methanol carbonylation on HMOR and Cu-HMOR by IR and solid-state NMR found that copper enhanced the formation rate of MA remarkably [79]. A Cu^+–CO complex was formed under reaction conditions (200–240 °C), and DME (in situ formed by methanol dehydration), rather than methanol and water, preferentially adsorbed on the Cu^+–CO site (Fig. 9). Therefore, the enhanced reaction rate might be ascribed to the attack of surface methyl group by the vicinal CO group involved in the Cu^+–CO complex, and the preferential co-adsorption of DME on Cu^+–CO site facilitated the attack of DME to acetyl group, resulting in the formation of MA as the primary product. However, solid-state NMR study also suggested that the role of Cu^+ is to stabilize DME and suppress the formation of hydrocarbons; CO adsorbed on Cu^+ did not participate in the carbonylation process, as introducing methanol to ^{13}CO adsorbed on Cu^+ site resulted in the formation of hydrocarbons, instead of the carbonylation product [80].

On the other hand, Cu^0, rather than Cu^+, was proposed to be responsible for the promotional effect in DME carbonylation [52]. As shown in Fig. 10, the space time yield of MA was positively correlated with the amount of Cu^0, but negatively related to the content of Cu^+, over a series of Cu/HMOR samples with different amount of Cu. The promoting role of Cu^0 in methanol and DME carbonylation was also supported by a recent DFT study on Cu/HZSM-5 [81], which predicted that the higher activity of Cu^0 probably originates from the strong electrostatic interaction between the nucleophilic CH_3^+–CO intermediate and the electrophilic Cu^0 site. In situ IR and DFT calculations further suggested a synergetic working model of Cu^0 and the neighboring Brønsted acid site [82]. DME adsorption and dissociation resulted in the formation of CH_3–Cu^0 and CH_3OH that adsorbed on the neighboring Brønsted acid site; the co-adsorption of CO on Cu° facilitated CO insertion into the CH_3–Cu^0 to generate a Cu–$COCH_3$ acetyl intermediate that further reacted with the CH_3OH adsorbed on the neighboring Brønsted acid site to produce MA (Fig. 11).

It seems that the reaction chemistry of Cu^0 and Cu^+ in zeolites with CO, DME, methanol, and the intermediates during DME carbonylation needs further clarification. For methanol carbonylation, Cu^+ benefits the adsorption and stabilization of the in situ formed DME, but the strongly adsorbed Cu^+–CO is not likely to participate in the formation of acetyl species. On the other hand, Cu^0 is most likely to play a promotional role in DME carbonylation, but its spatial location in the pore systems of HMOR and chemical interaction with the Brønsted acid site needs to be clarified.

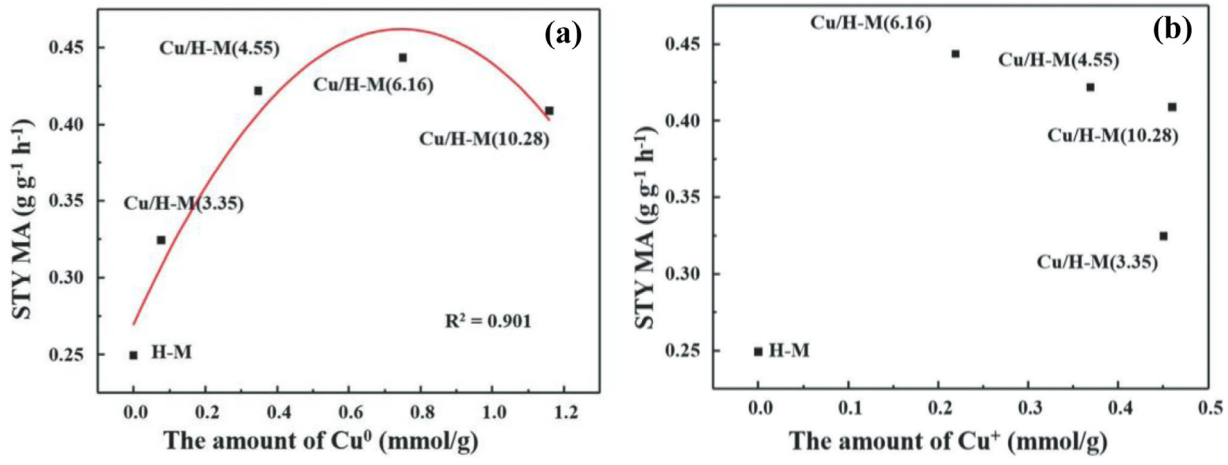

Fig. 10. The correlation of MA yield with Cu^0 (a) and Cu^+ (b) on Cu/HMOR catalysts [52].

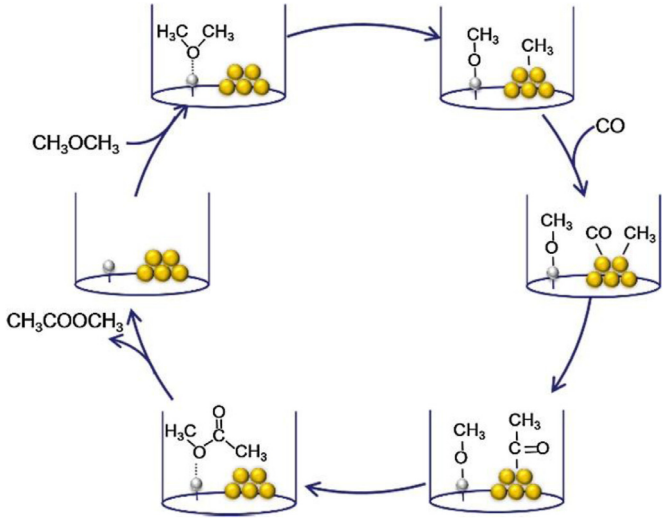

Fig. 11. Proposed reaction mechanism for DME carbonylation on Cu/HMOR catalyst. The proton and Cu° cluster are represented by white and yellow balls, respectively [82].

5. Deactivation of HMOR

5.1. Coke deposition in 12-MR pores

DME carbonylation occurs exclusively in the 8-MR pores of HMOR and HFER. HMOR is characterized by a higher activity toward MA formation but suffers from a rapid deactivation, while HFER (typically HZSM-35) showed a relatively lower activity but a higher durability [33]. Coke formation was confirmed to inhibit the access of DME to the active sites in the 8-MR pores. It is highly possible that aromatic compounds, which was regarded as the precursor for coke formation, was formed more easily in the large 12-MR pore of HMOR (6.5×7 Å) than that in the smaller 10-MR pore (5.4×4.2 Å) of HZSM-35. Theoretical calculations indicated that reaction of surface methyl with DME to form trimethyl oxonium cation (TMO^+) undergoes with a much lower energy barrier around 28–46 kJ mol^{-1} on T sites (T1, T2 and T4) in the 12-MR channels than that for CO insertion (around 100 kJ mol^{-1}) [32]. TMO^+ has been generally regarded as a precursor for the formation of hydrocarbons [83], which is kinetically favored in the 12-MR channel of HMOR and thus possibly results in coke formation. Analysis on deactivation kinetics over HMOR showed that formation of coke was kinetically increased by both DME and CO [84]. A kinetic equation for deactivation was proposed by modeling the experimental and calculated data of DME, CO and MA concentrations in the reaction system as a function of time on stream:

$$-\frac{da}{dt} = k_d y_{DME} y_{CO} a^d$$

where k_d is the kinetic constant for deactivation; y_{DME} and y_{CO} are the mole fractions of DME and CO in the reaction stream, respectively; a is the relative activity of MA formation at time t to the initial rate, which defined as $a = \frac{r_{MA}}{(r_{MA})_0}$; d is the order of deactivation.

Combining the experimental results and theoretical analysis, it seems that the acid sites in the 12-MR channel of HMOR catalyzed several side reactions for coke formation, including condensation of MA as well as other intermediates to oxygen-containing aggregates (soft coke), DME to hydrocarbons, hydrocarbons to aromatics and finally to coke. All these byproducts or undesired oligomers block the pores or the active sites and therefore resulted in significant deactivation. However, it should be noticed that the 12-MR channel is essential for DME diffusion to access and MA diffusion out of the active sites within the 8-MR pores. As suggested by DFT calculations [85], the interconnection of 8-MR and 12-MR pores of MOR favored a fasted diffusion of MA, as compared with zeolites of other topologies (FER, GON, ATS, and IRN). The positive role of the 12-MR pores was also experimentally proved by ^{129}Xe NMR results, which directly showed that Xe enter the 8-MR pores only through the 12-MR channels [36]. As the kinetic diameter of DME (4.307 Å) is even larger than that of Xe (4.047 Å) [86], it is most likely that DME accesses the active sites in the 8-MR pores only through the 12-MR pores.

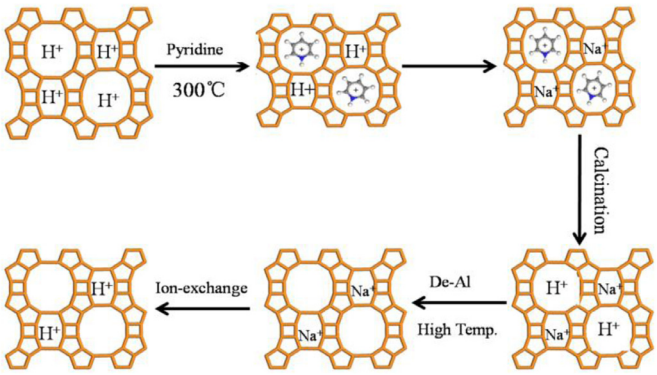

Fig. 12. Selective removal of Al atoms in the 12-MR channel of MOR [90].

5.2. Modification of acid sites in 12-MR pores

Based on the functions of acid sites in different pores of HMOR during DME carbonylation, several strategies have been proposed to eliminate or poison the acid sites in the 12-MR pores. Selective pre-adsorption of pyridine (Py) on the acid sites in the 12-MR channel was demonstrated to enhance the lifetime of HMOR for DME carbonylation [34]. The precondition was that pyridine adsorption must be done at an appropriate temperature range, for example 300 °C, which is necessarily higher than the reaction condition (200 °C). It was experimentally proved that pyridine did not enter the 8-MR pores of HMOR and thus kept the active sites for DME carbonylation unchanged or undisturbed; while those diffused into the 12-MR channels passivated the acid sites and thus inhibited coke deposition. This approach was subjected to intensive investigations on HMOR catalysts for DME or methanol carbonylation [36,87–89]. An NMR study on the effect of adsorption quantity of pyridine on the activity and stability of HMOR indicated that pyridine adsorbed in the 12-MR pore of HMOR decreased the self-diffusion efficiency of molecules, which lowered DME conversion rate, but dramatically enhanced the catalytic stability [36]. The positive role of pyridine adsorption in the stability of DME carbonylation was also related to the Si/Al ratio of HMOR. Higher Al density in the 12-MR pores decreased pyridine adsorption strength and led to an easier desorption of pyridine during reaction, which consequently resulted in a fast deactivation of the catalyst [89].

Because of the possible desorption of pyridine under the reaction conditions, even if properly pre-adsorbed, selective removal of acid sites (Al sites) the 12-MR channel of HMOR was developed [90]. As shown in Fig. 12, pyridine was firstly adsorbed in the 12-MR channel of HMOR to prevent H^+ from being ion-exchanged in the following step that selectively introduced Na^+ into the 8-MR pores; calcination in air at 500 °C yielded MOR with H^+ in the 12-MR pores and Na^+ in the 8-MR pores; steam treatment of this sample at 750 °C preferentially removed 86% of framework Al atoms in the 12-MR channels while retained those in the 8-MR pores. Catalytic stability of such a catalyst was dramatically

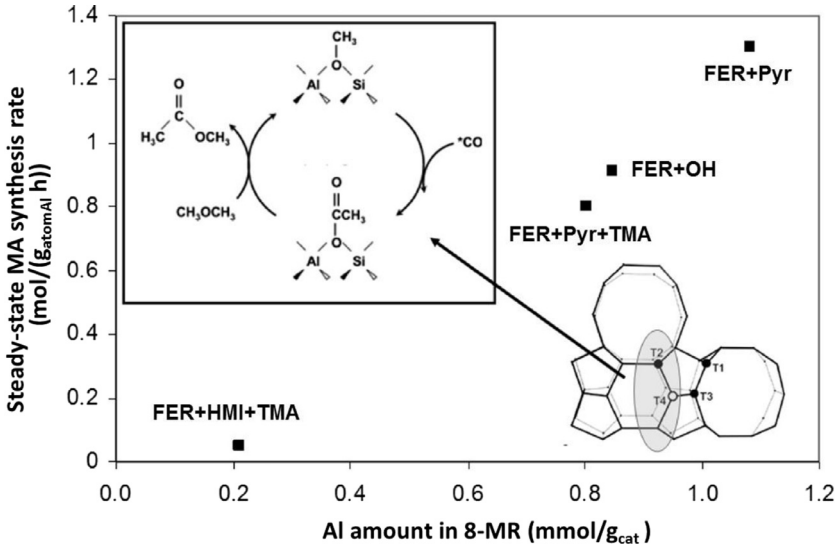

Fig. 13. Production rate of methyl acetate as a function of the amount of acid sites in the 8-MR pores of ferrierites [67].

improved during DME carbonylation. Here, it should be noted that routine dealumination procedures, such as washing with mineral acids, did not work for this purpose, because it would cause preferential removal of framework Al atoms at T3 and T4 sites [91,92], thus lower the activity for MA formation. Dealumination with oxalic acid and ammonium hexafluorosilicate also weakened the strength of Brønsted acid sites in the 8-MR pore of HMOR, and hence dramatically lowered the formation rate of MA [93].

6. Acid site and pore engineering

6.1. Population of acid sites

A more effective and straightforward route to enhance the activity of zeolites for DME carbonylation is to enrich the acid sites in the 8-MR pores. It has been shown that appropriate combination of structure directing agents (SDAs) could change the siting of Al atoms in the 8-MR and 10-MR channels of HFER [67]. By using pyrrolidine as the SDA, either combining with tetramethylammonium (TMA) or not, more than 80% Al atoms were introduced into the 8-MR pores of HFER; while the combination of hexamethyleneimine (HMI) with TMA resulted in merely 27% Al atoms in the 8-MR pores. The NH_2^+ group of protonized HMI (by HF) has a stronger ability to interact with Al than TMA^+, its preferable location in the large pores induced more Al atoms into the 10-MR pores. When the samples were tested for DME carbonylation, a linear increase in MA formation rate with the enrichment of Al atoms in the 8-MR pores was obtained (Fig. 13).

The directing effect of SDAs on Al population in the 8-MR and 12-MR pores of HMOR was also observed. Using HMI as the SDA for the hydrothermal synthesis of mordenite (with a Si/Al ratio of 11.8) resulted in 72.7% Al atoms in the 8-MR pores, while tetraethylammonium hydroxide (TEAOH) induced 65.9% Al atoms in the 8-MR pore [37]. HMI, with a kinetic diameter of 0.76 nm, played a pore filling role in MOR crystallization: it blocked the incorporation of Al in the 12-MR pores and hence resulted in more Al population in the 8-MR pores. Using TEAOH as SDA for MOR synthesis by an amine vapor assisted dry-gel conversion method introduced 75% of Al atoms into the 8-MR pores [88]. As generally expected, the enrichment of Al atoms in the 8-MR pores of HMOR has essentially increased the formation rate of MA during DME carbonylation.

6.2. Pore engineering

Diffusion limitation of reactants/products is a major drawback for the traditional micro-sized zeolites. Creating mesopores inside the zeolite crystals is frequently used to enhance the diffusion efficiency. Alkaline desilication is commonly adapted to create mesopores, especially for high silica zeolites. Mild alkaline treatment removed amorphous debris particles on FER (ZSM-35) crystal surface and generated fissures on the crystals, which enhanced mass transfer. The conversion of DME increased moderately from 37% over the original ZSM-35 to 44% after alkaline treatment [43]. Similarly, alkaline treatment of HMOR enhanced the activity and stability of DME carbonylation, possibly due to the generation of mesopores inside the zeolite crystals [94,95]. Upon treatment with 0.2 M aqueous NaOH solution at 65 °C for 0.5 h for HMOR (Si/Al ratio of 20), the formation rate of acetyls increased from 0.133 g mL_{cat}^{-1} h^{-1} to 0.294 g mL_{cat}^{-1} h^{-1} at time on stream of 140 h [94]. However, it is worth noting that alkaline treatment of mordenite might also remove the strong acid sites, possibly in the 8-MR pores, and decrease the number of active sites for DME carbonylation. Fortunately, it was recently reported that alkaline treatment of the as-synthesized (uncalcined) mordenite that still contained the template (tetraethyl ammonium bromide) could protect the micropores and the acid sites in the 8-MR side pockets but also created a substantial fraction of mesopores. The resulting HMOR catalyst showed enhanced stability without obvious decrease in the activity for DME carbonylation; whereas alkaline treatment of the calcined sample resulted in a dramatic decrease in the formation rate of MA [95].

Decreasing the crystal size of zeolites to nanometer level is another approach to shorten the micropore/channel length and thus promote intracrystal diffusion efficiency. This largely relies on the careful optimization of the synthetic parameters and the proper use of SDAs, with a well balance between the crystallinity and the particle size. For example, the crystallite size of HMOR was reduced to 50–100 nm by using $(CH_3CH_2)_3N^+–(CH_2)_5–N^+(CH_2CH_3)_3Br_2$ (Et_6-diquat-5) as the SDA under dynamic crystallization conditions [96]. The catalyst activity and stability for DME carbonylation was greatly enhanced as compared to the micro-sized HMOR (2–6 μm) with a similar Si/Al ratio; the formation rate of MA increased by 3 times while the deactivation rate constant (k_d) decreased from 0.21 h^{-1} to 0.08 h^{-1} (Fig. 14). Nanocrystal-assembled hierarchical mordenite was

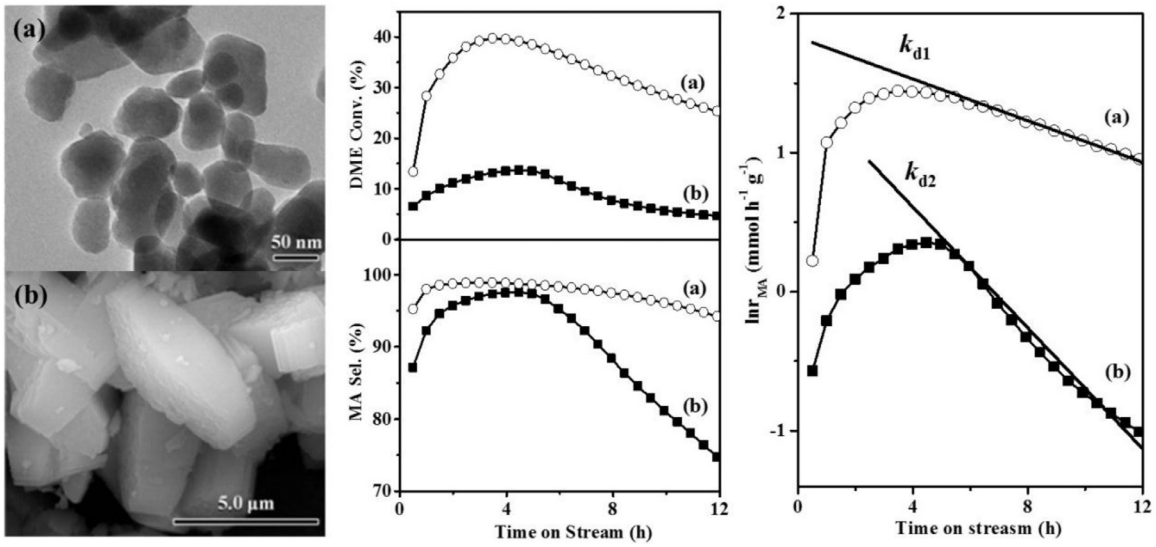

Fig. 14. SEM/TEM images and DME carbonylation performance of nano-sized (a) and micro-sized (b) HMOR samples [96].

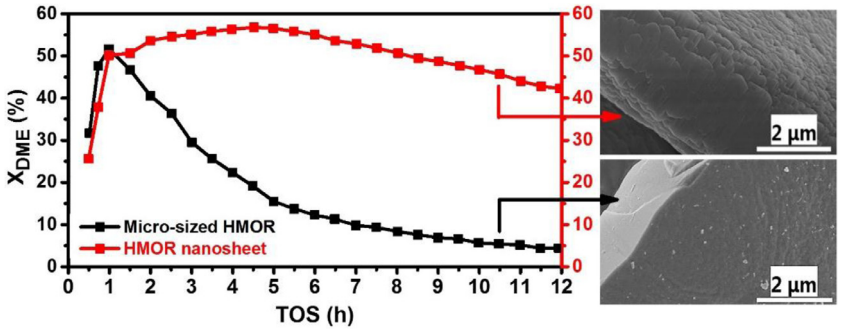

Fig. 15. DME carbonylation performance and SEM images of HMOR nanosheets and micro-sized HMOR [35].

hydrothermally fabricated by using TEAOH as the crystal-forming agent and a diquaternary ammonium surfactant as the crystal-growth inhibiting agent [97]. The 10–20 μm spherical particles were assembled by 20–50 nm crystals, gave a higher DME conversion (40%) than that over the commercial HMOR sample (30%) with a similar Si/Al ratio. The apparently enhanced activity was ascribed to the shortened diffusion lengths.

Shape mediation of zeolite particles by reducing the size of a specific crystal dimension to the nanometer scale while keeping other dimensions at the micrometer scale was developed recently. This strategy could significantly reduce the diffusion length in the nanometer dimension and reserve the high crystallinity of zeolite in the micrometer dimensions on the same crystal. MFI nanosheets set a typical example in this context. MFI (ZSM-5) nanosheets with a single-unit-cell thickness of 2 nm along the b-axis were successfully synthesized under hydrothermal conditions by using a diquaternary ammonium surfactant as the SDA [98]. Self-pillared nanosheets of MFI/MEL intergrowths with a thickness of 2 nm have been hydrothermally synthesized via a repetitive branching pattern using tetrabutylphosphonium hydroxide as the SDA [99]. The short channels along the b-axis of these nanosheets greatly promoted their performances for methanol to gasoline, methanol to propylene, and self-etherification of benzyl alcohol to dibenzyl ether [98,100].

For DME carbonylation, hierarchical HMOR assemblies, with a sheet thickness of 50–100 nm, showed obviously enhanced stability as compared to a micro-sized HMOR (~ 3 μm) with a similar Si/Al ratio of 5–6 (Fig. 15) [35]. A similar enhancing effect of nanosheet-assembled hierarchical HMOR, synthesized by using polyethylene glycol as the template, was also evidenced recently [101]. HMOR nanosheets with shortened 12-MR channels was hydrothermally synthesized by using a single quaternary ammonium surfactant as the SDA (Fig. 16). The increased formation rate of MA during DME carbonylation was assigned to the easier molecular diffusion

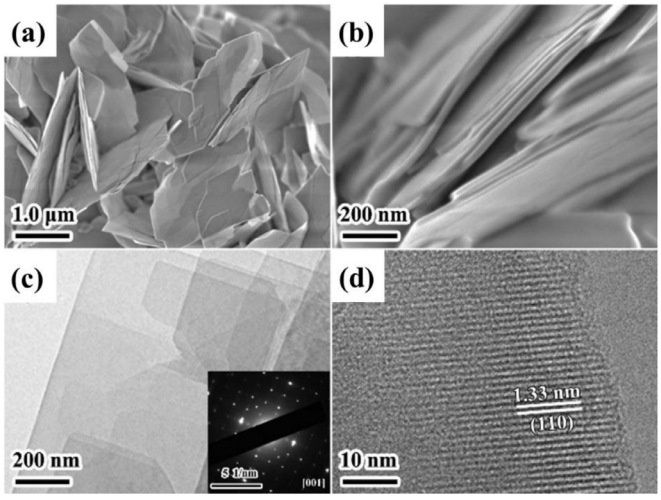

Fig. 16. SEM/TEM images of the HMOR nanosheets; the inset in (c) is the selected area electron diffraction (SAED) pattern viewed along the [001] direction [45].

inside the zeolite crystals [45]. In principle, the short 12-MR channel in HMOR nanosheet has a long-range crystal integrity in the a-b plane, so the structure of the 8-MR side pockets remains unchanged. Such nanostructured HMOR represents one of the most potential ways to promote the efficiency for DME carbonylation by essentially enhancing the activity and stability.

7. Concluding remarks

Zeolite-catalyzed DME carbonylation to MA represents a novel and efficient route for building C–C bond in the field of C1 chemistry. Intensive experimental studies and theoretical calculations have convincingly evidenced the formation mechanism of acetyl as the key intermediate: CO insertion to surface methyl on the acid sites in the 8-MR pores of zeolites, as the rate-determining step in the reaction network. Modification of the zeolites with transition metals often resulted in more active, and possibly stable, catalysts for DME carbonylation. The metal components were experimentally verified to enhance the adsorption and activation of CO, but the working mechanism is far from being understood. Coke formation was catalyzed by the acid sites in the larger pores of HMOR or HFER, and several strategies were developed to weaken or eliminate the acid sites in the larger pores. Pre-adsorption of pyridine to suppress the acid sites in the 12-MR channel of HMOR seemed to be a reliable and effective approach by far. However, the chemical nature of the accumulated soft cokes (oligomerized oxygenates) and their formation mechanism within the entire zeolite crystals remains unclear. Simultaneously, lowering the size and tailoring the shape of zeolite crystals have been proved to significantly enhance the diffusion efficiency and thus promote the catalytic stability, but the synthesis of these nanostructured zeolites is challenging. Overall, the ultimate goal for the development of active and stable catalysts for DME carbonylation would rely largely on properly manipulating the acid site population and tailoring the size/shape of zeolites: (a) preferential location of most Al atoms in the 8-MR pores other than the 10- or 12-MR pores; (b) considerable decrease in the diffusion length of molecules within zeolite crystals; and (c) selective doping with transition metals in the 8-MR pore of the nanostructured zeolites to form site-syngenetic catalysis for the activation of DME and CO.

Acknowledgments

This work is supported by the National Natural Science Foundation of China (Grant no. 20973166).

References

[1] C. Higman, S. Tam, Chem. Rev. 114 (2014) 1673–1708.
[2] K. Cheng, J. Kang, D.L. King, V. Subramanian, C. Zhou, Q. Zhang, Y. Wang, Adv. Catal. 60 (2017) 125–208.
[3] G. Bozzano, F. Manenti, Prog. Energy Combust. Sci. 56 (2016) 71–105.
[4] K. Saravanan, H. Ham, N. Tsubaki, J.W. Bae, Appl. Catal. B 217 (2017) 494–522.
[5] J. Sun, G. Yang, Y. Yoneyama, N. Tsubaki, ACS Catal. 4 (2014) 3346–3356.
[6] V. Subramani, S.K. Gangwal, Energy Fuels 22 (2008) 814–839.
[7] R.G. Herman, Catal. Today 55 (2000) 233–245.
[8] N. Yoneda, S. Kusano, M. Yasui, P. Pujado, S. Wilcher, Appl. Catal. A 221 (2001) 253–265.
[9] J. Zhou, Y. Zhao, J. Zhang, Y. Wang, O.Y. Gutiérrez, S. Wang, Z. Li, P. Jin, S. Wang, X. Ma, J.A. Lercher, Chem. Commun. 54 (2018) 8818–8821.
[10] B. Wang, X. Wang, G. Xu, Nat. Gas Chem. Ind. 38 (2013) 79–83.
[11] X. Xu, Y. Liu, F. Zhang, W. Di, Y. Zhang, Catal. Today 298 (2017) 61–68.
[12] X. San, Y. Zhang, W. Shen, N. Tsubaki, Energy Fuels 23 (2009) 2843–2844.
[13] X. Li, X. San, Y. Zhang, T. Ichii, M. Meng, Y. Tan, N. Tsubaki, ChemSusChem 3 (2010) 1192–1199.
[14] X. Gao, B. Xu, G. Yang, X. Feng, Y. Yoneyama, U. Taka, N. Tsubaki, Catal. Sci. Technol. 8 (2018) 2087–2097.
[15] X. Feng, P. Zhang, Y. Fang, W. Charusiri, J. Yao, X. Gao, Q. Wei, P. Reubroycharoen, T. Vitidsant, Y. Yoneyama, G. Yang, N. Tsubaki, Catalysis Today (2019). https://doi.org/10.1016/j.cattod.2019.02.054.
[16] A. Haynes, Adv. Catal. 53 (2010) 1–45.
[17] H. Koch, W. Haaf, Justus Liebigs Ann. Chem. 618 (1958) 251–266.
[18] K. Fujimoto, T. Shikada, K. Omata, H. Tominaga, Chem. Lett. (1984) 2047–2050.
[19] B. Ellis, M.J. Howard, R.W. Joyner, K.N. Reddy, M.B. Padley, W.J. Smith, Stud. Surf. Sci. Catal. 101 (1996) 771–779.
[20] R.W. Wegman, Chem. Commun. (1994) 947–948.
[21] G.G. Volkova, L.M. Plyasova, A.N. Salanov, G.N. Kustova, T.M. Yurieva, V.A. Likholobov, Catal. Lett. 80 (2002) 175–179.
[22] M.V. Luzgin, M.S. Kazantsev, G.G. Volkova, W. Wang, A.G. Stepanov, J. Catal. 277 (2011) 72–79.
[23] A. Sardesai, S. Lee, T. Tartamella, Energy Sources 24 (2002) 301–317.
[24] G.G. Volkova, L.M. Plyasova, L.N. Shkuratova, A.A. Budneva, E.A. Paukshtis, M.N. Timofeeva, V.A. Likholobov, Stud. Surf. Sci. Catal. 147 (2004) 403–408.
[25] H. Shen, Y. Li, S. Huang, K. Cai, Z. Cheng, J. Lv, X. Ma, Catal Today (2018). https://doi.org/10.1016/j.cattod.2018.04.001.
[26] M.V. Luzgin, M.S. Kazantsev, W. Wang, A.G. Stepanov, J. Phys. Chem. C 113 (2009) 19639–19644.
[27] M.S. Kazantsev, M.V. Luzgin, A.G. Stepanov, J. Phys. Chem. C 117 (2013) 11168–11175.
[28] M.V. Luzgin, M.S. Kazantsev, G.G. Volkova, A.G. Stepanov, J. Catal. 308 (2013) 250–257.
[29] G.G. Volkova, E.A. Paukshtis, Catal. Sustain. Energy 4 (2018) 59–61.
[30] P. Cheung, A. Bhan, G.J. Sunley, E. Iglesia, Angew. Chem. Int. Ed. 45 (2006) 1617–1620.
[31] P. Cheung, E. Iglesia, J.G. Sunley, A. Bhan, D.J. Law, US patent, US2006287551(A1).
[32] M. Boronat, C. Martinez-Sanchez, D. Law, A. Corma, J. Am. Chem. Soc. 130 (2008) 16316–16323.
[33] J. Liu, H. Xue, X. Huang, Y. Li, W. Shen, Catal. Lett. 139 (2010) 33–37.
[34] J. Liu, H. Xue, X. Huang, P.-H. Wu, S.-J. Huang, S.-B. Liu, W. Shen, Chin. J. Catal. 31 (2010) 729–738.
[35] Y. Liu, N. Zhao, H. Xian, Q. Cheng, Y. Tan, N. Tsubaki, X. Li, ACS Appl. Mater. Interfaces 7 (2015) 8398–8403.
[36] T. He, X. Liu, S. Xu, X. Han, X. Pan, G. Hou, X. Bao, J. Phys. Chem. C 120 (2016) 22526–22531.
[37] M. Wang, S. Huang, J. Lu, Z. Cheng, Y. Li, S. Wang, X. Ma, Chin. J. Catal. 37 (2016) 1530–1538.
[38] A.A.C. Reule, N. Semagina, ACS Catal. 6 (2016) 4972–4975.
[39] S.Y. Park, C.-H. Shin, J.W. Bae, Catal. Commun. 75 (2016) 28–31.
[40] X. Li, X. Chen, Z. Yang, X. Zhu, S. Xu, S. Xie, S. Liu, X. Liu, L. Xu, Microporous Mesoporous Mater. 257 (2018) 79–84.
[41] N. Zhao, Q. Cheng, S. Lyu, L. Guo, Y. Tian, T. Ding, J. Xu, X. Ma, X. Li, Catal. Today (2019). https://doi.org/10.1016/j.cattod.2019.01.013.
[42] E. Iglesia, J.G. Sunley, D.J. Law, A. Bhan, WIPO patent, WO2008073096(A1).
[43] X. Li, X. Liu, S. Liu, S. Xie, X. Zhu, F. Chen, L. Xu, RSC Adv. 3 (2013) 16549–16557.
[44] H. Xue, X. Huang, E. Ditzel, E. Zhan, M. Ma, W. Shen, Ind. Eng. Chem. Res. 52 (2013) 11510–11515.
[45] M. Ma, X. Huang, E. Zhan, Y. Zhou, H. Xue, W. Shen, J. Mater. Chem. A 5 (2017) 8887–8891.
[46] X. Feng, J. Yao, H. Li, Y. Fang, Y. Yoneyama, G. Yang, N. Tsubaki, Chem. Commun. 55 (2019) 1048–1051.
[47] W. Fan, J. Xu, W. Yan, Y. Wei, J. Li, J. Wang, M. Dong, J. Yu, R. Xu, Chinese patent, CN108586247(A)
[48] J.E. Lewis, C.C. Freyhardt, M.E. Davis, J. Phys. Chem. 100 (1996) 5039–5049.
[49] Evert Jan Ditzel, David John Law, M.S. Roberts, US patent, US20100130771(A1).
[50] Evert Jan Ditzel, Andre Harmen Sijpkes, J.G. Sunley, US patent, US20100121098(A1).
[51] S. Wang, W. Guo, L. Zhu, H. Wang, K. Qiu, K. Cen, J. Phys. Chem. C 119 (2015) 524–533.
[52] H. Zhan, S. Huang, Y. Li, J. Lv, S. Wang, X. Ma, Catal. Sci. Technol. 5 (2015) 4378–4389.
[53] H. Zhou, W. Zhu, L. Shi, H. Liu, S. Liu, S. Xu, Y. Ni, Y. Liu, L. Li, Z. Liu, Catal. Sci. Technol. 5 (2015) 1961–1968.
[54] M. Ma, E. Zhan, X. Huang, N. Ta, Z. Xiong, L. Bai, W. Shen, Catal. Sci. Technol. 8 (2018) 2124–2130.
[55] X. Zhang, Y. Li, S. Qiu, T. Wang, M. Ding, Q. Zhang, L. Ma, Y. Yu, Chin. J. Chem. Phys. 26 (2013) 77–82.
[56] A.A.C. Reule, J. Shen, N. Semagina, ChemPhysChem 19 (2018) 1500–1506.
[57] A.A.C. Reule, V. Prasad, N. Semagina, Microporous Mesoporous Mater. 263 (2018) 220–230.
[58] Z. Zhang, N. Zhao, K. Ma, Q. Cheng, J. Zhang, L. Zheng, Y. Tian, X. Li, Chin. Chem. Lett. 30 (2019) 513–516.
[59] P. Cheung, A. Bhan, G.J. Sunley, D.J. Law, E. Iglesia, J. Catal. 245 (2007) 110–123.
[60] X. Chen, M.L. Neidig, R. Tuinstra, A. Malek, J. Phys. Chem. Lett. 1 (2010) 3012–3015.
[61] H. Zhou, W. Zhu, L. Shi, H. Liu, S. Liu, Y. Ni, Y. Liu, Y. He, S. Xu, L. Li, Z. Liu, J. Mol. Catal. A Chem. 417 (2016) 1–9.
[62] B. Li, J. Xu, B. Han, X. Wang, G. Qi, Z. Zhang, C. Wang, F. Deng, J. Phys. Chem. C 117 (2013) 5840–5847.
[63] T. He, P. Ren, X. Liu, S. Xu, X. Han, X. Bao, Chem. Commun. 51 (2015) 16868–16870.
[64] A. Zecchina, G. Spoto, S. Bordiga, PCCP 7 (2005) 1627–1642.
[65] M. Boronat, C. Martinez, A. Corma, PCCP 13 (2011) 2603–2612.

[66] A. Bhan, A.D. Allian, G.J. Sunley, D.J. Law, E. Iglesia, J. Am. Chem. Soc. 129 (2007) 4919–4924.
[67] Y. Roman-Leshkov, M. Moliner, M.E. Davis, J. Phys. Chem. C 115 (2011) 1096–1102.
[68] M.W. Anderson, J. Klinowski, J. Am. Chem. Soc. 112 (1990) 10–16.
[69] C.M. Zicovich-Wilson, A. Corma, P. Viruela, J. Phys. Chem. 98 (1994) 10863–10870.
[70] A. Bhan, E. Iglesia, Acc. Chem. Res. 41 (2008) 559–567.
[71] R. Gounder, E. Iglesia, Acc. Chem. Res. 45 (2012) 229–238.
[72] D.B. Rasmussen, J.M. Christensen, B. Temel, F. Studt, P.G. Moses, J. Rossmeisl, A. Riisager, A.D. Jensen, Angew. Chem. Int. Ed. 54 (2015) 7261–7264.
[73] R. Gounder, E. Iglesia, Chem. Commun. 49 (2013) 3491–3509.
[74] P. Feng, G. Zhang, K. Zang, X. Li, L. Xu, X. Chen, Chem. Phys. Lett. 684 (2017) 279–284.
[75] J. Kim, H. Ham, H.S. Jung, Y. Wang, Y. He, N. Tsubaki, S.J. Cho, G.Y. Han, J.W. Bae, Catal. Sci. Technol. 8 (2018) 3060–3072.
[76] H.S. Jung, H. Ham, J.W. Bae, Catal. Today (2019). https://doi.org/10.1016/j.cattod.2019.02.042.
[77] P. Feng, G. Zhang, X. Chen, K. Zang, X. Li, L. Xu, Appl. Catal., A 557 (2018) 119–124.
[78] D.B. Rasmussen, J.M. Christensen, B. Temel, F. Studt, P.G. Moses, J. Rossmeisl, A. Riisager, A.D. Jensen, Catal. Sci. Technol. 7 (2017) 1141–1152.
[79] T. Blasco, M. Boronat, P. Concepcion, A. Corma, D. Law, J.A. Vidal-Moya, Angew. Chem. Int. Ed. 46 (2007) 3938–3941.
[80] L. Zhou, S. Li, G. Qi, Y. Su, J. Li, A. Zheng, X. Yi, Q. Wang, F. Deng, Solid State Nucl. Magn. Reson. 80 (2016) 1–6.
[81] S. Wang, S. Li, L. Zhang, Z. Qin, Y. Chen, M. Dong, J. Li, W. Fan, J. Wang, Catal. Sci. Technol. 8 (2018) 3193–3204.
[82] Y. Li, S. Huang, Z. Cheng, S. Wang, Q. Ge, X. Ma, J. Catal. 365 (2018) 440–449.
[83] U. Olsbye, S. Svelle, K.P. Lillerud, Z.H. Wei, Y.Y. Chen, J.F. Li, J.G. Wang, W.B. Fan, Chem. Soc. Rev. 44 (2015) 7155–7176.
[84] Z. Cheng, S. Huang, Y. Li, J. Lv, K. Cai, X. Ma, Ind. Eng. Chem. Res 56 (2017) 13618–13627.
[85] Z. Liu, X. Yi, G. Wang, X. Tang, G. Li, L. Huang, A. Zheng, J. Catal. 369 (2019) 335–344.
[86] J.R. Li, R.J. Kuppler, H.C. Zhou, Chem. Soc. Rev. 38 (2009) 1477–1504.
[87] Y. Ni, L. Shi, H. Liu, W. Zhang, Y. Liu, W. Zhu, Z. Liu, Catal. Sci. Technol. 7 (2017) 4818–4822.
[88] L. Li, Q. Wang, H. Liu, T. Sun, D. Fan, M. Yang, P. Tian, Z. Liu, ACS Appl. Mater. Interfaces 10 (2018) 32239–32246.
[89] Y. Li, Q. Sun, S. Huang, Z. Cheng, K. Cai, J. Lv, X. Ma, Catal. Today 311 (2018) 81–88.
[90] H. Xue, X. Huang, E. Zhan, M. Ma, W. Shen, Catal. Commun. 37 (2013) 75–79.
[91] P. Bodart, J.B. Nagy, G. Debras, Z. Gabelica, P.A. Jacobs, J. Phys. Chem. 90 (1986) 5183–5190.
[92] A.A.C. Reule, J.A. Sawada, N. Semagina, J. Catal. 349 (2017) 98–109.
[93] K. Cai, S. Huang, Y. Li, Z. Cheng, J. Lv, X. Ma, ACS Sus. Chem. Eng. 7 (2019) 2027–2034.
[94] Gareth Gerald Armitage, Bogdan Costin Gagea, David John Law, J.G. Sunley, US papent, US20120078005(A1).
[95] X. Wang, R. Li, C. Yu, Y. Liu, L. Zhang, C. Xu, H. Zhou, Fuel 239 (2019) 794–803.
[96] H. Xue, X. Huang, E. Ditzel, E. Zhan, M. Ma, W. Shen, Chin. J. Catal. 34 (2013) 1496–1503.
[97] Y. Yuan, L. Wang, H. Liu, P. Tian, M. Yang, S. Xu, Z. Liu, Chin. J. Catal. 36 (2015) 1910–1919.
[98] M. Choi, K. Na, J. Kim, Y. Sakamoto, O. Terasaki, R. Ryoo, Nature 461 (2009) 246–249.
[99] X.Y. Zhang, D.X. Liu, D.D. Xu, S. Asahina, K.A. Cychosz, K.V. Agrawal, Y. Al Wahedi, A. Bhan, S. Al Hashimi, O. Terasaki, M. Thommes, M. Tsapatsis, Science 336 (2012) 1684–1687.
[100] L. Emdadi, Y. Wu, G. Zhu, C.-C. Chang, W. Fan, T. Pham, R.F. Lobo, D. Liu, Chem. Mater. 26 (2014) 1345–1355.
[101] X. Wang, R. Li, C. Yu, L. Zhang, C. Xu, H. Zhou, Microporous Mesoporous Mater. 274 (2019) 227–235.